



Research paper

A study on RCFST column instability modes

Zhengran Lu¹, Chao Guo²

Abstract: In this work, the instability damage modes of yield state of a steel tube at the tension side of a rectangular steel tube-confined concrete (RCFST) column under eccentric compression were classified into two types based on the coupling effect of slenderness ratio (λ) and eccentricity ratio (γ). The two types include the unilateral compression yield failure mode with a smaller value of γ and tensile and compressive yield failure modes on both column sides with a larger value of γ . Further, the parametric analyses were performed by employing the finite element (FE) method and the analytical analysis to test 16 groups of RCFST columns by varying the γ value with different λ values. It was observed that the results of the analysis for the mechanical properties like the responses of load-strain ($P-\varepsilon$) and RCFST column instability modes correlated well with the results obtained in the experiments. Furthermore, the proposed theoretical method could be used to investigate the roles of γ as a controller against the instability in RCFST columns when compared with λ .

Keywords: rectangular steel tube-confined concrete, eccentricity ratio, slenderness ratio, instability, FE analysis, theoretical analysis

¹Prof., PhD., School of Civil Engineering, Shenyang Jianzhu University, Shenyang 110168, China, e-mail: luzhengran@sjzu.edu.cn, ORCID: 0000-0002-4870-7430

²Prof., PhD., School of Civil Engineering, Shenyang Jianzhu University, Shenyang 110168, China, e-mail: guochao@sjzu.edu.cn, ORCID: 0000-0001-9389-731X

1. Introduction

The rectangular steel tube-confined concrete (RCFST) greatly enhances column strength and decreases column sectional area [1]. However, it does not contribute to complete steel tube restraint effect on concrete core columns (CCC) when compared to the circular steel tubes [2, 3]. In addition, the steel tubes were susceptible to undergo local buckling at the middle under compressive action [4]. RCFST long column compressibility and bending stability were considered to be a nonlinear problem due to the relation between column end constraints slenderness ratio (λ), and eccentricity ratio (γ) [5]. Under such conditions, where the steel tubes were subjected to local buckling and CCC constraint loss, long columns were found to lose their stability significantly [6]. Hence, performing a detailed study on RCFST instability modes is essential in order to evaluate γ and λ effects on RCFST [7, 8]. Also, RCFST long column in-plane static instability modes also must be investigated [9]. The conditions of RCFST long column critical stability were calculated using length, inertia moment, and elastic modulus [10, 11]. Despite this, it was assumed that the inertia moments and elastic moduli steel and concrete had unified values and material difference was not considered while calculating codes EC4 [12], AISC 360 [13] and GB 50936 [14] peak-load values. Concrete and steel tube contributions towards RCFST critical were considered separately in the composite theory, however, it was also essential that CCC and steel tubes simultaneously bear the load [15].

However, concrete and steel did not simultaneously bear the load during actual instability process. In addition, steel yield strain was high ($\varepsilon_p = 0.002$) whereas concrete tensile strains were very low ($\varepsilon_c = 0.0007$) [16]. During the vending deformation of the RCFST columns, the CCC would delaminate from steel tubes and move into final failure stage and lose the bearing function [17]. Moreover, the RCFST columns had more complicated instability modes along with many defects [18, 19]. This was verified with various investigations and numerical analyses. These studies showed that the instability of RCFST long columns was calculated using the local buckling of steel tubes and the cracking of concrete [20].

By using 16 groups of high strength RCFST long columns, Li et al. [21, 22] performed numerical and experimental parametric analyses including the detailed analysis under the conditions of $\gamma = 0.13, 0.23, 0.33,$ and 0.43 with $\lambda = 10.4, 23.1, 34.6,$ and $46.2,$ respectively. However, the numerical parametric analyses in [21, 22] could not reveal the local buckling instability mechanism of steel tubes in RCFST columns, because the steel tube was simulated with the solid element type.

In order to address this issue, initially, the FE analysis using ABAQUS software was performed to obtain the longitudinal stresses of the steel tube with shell-type elements, and the compression damage factor in the middle section of CCC in RCFST columns. Further, the unilateral compression and the bilateral compression-tension modes combined with different γ and λ values were obtained using the numerical parametric analyses. Subsequently, in order to express the instability modes in a dimensionless normalized manner, implicit function equations were determined using the modified Jezek method. Finally, with the Maple program, parametric coupling effect analyses of λ and γ on RCFST long column system instability modes were performed for the validation of the developed analytical analysis method.

2. Experimental analysis

2.1. Specimen summarized

In order to investigate eccentricity ($\gamma = e_0/B = 0.13\text{--}0.43$) and slenderness ($\lambda = 10.4\text{--}46.2$) ratio effects on RCFST column behaviors, 32 specimens in 16 groups with different eccentric distances ($e_0 = 20\text{--}65$ mm) and lengths ($L = 450\text{--}2000$ mm) were experimented [21, 22], and the obtained parameters are illustrated in Table 1, where the $\lambda = \frac{2\sqrt{3}L}{B}$ [23, 24]. In addition, the thickness (t) and outer width (B) of square steel tubes, respectively, were 4 and 150 mm. Experimental setup and specimen details are presented in Fig. 1.

Table 1. Parameters of 16 RCFST column groups

Phase	E (GPa)	μ	f_{ck} (MPa)	f_{sy} (MPa)	f_{su} (MPa)	Ref
Concrete	41.8	0.2	110.5			[21, 22]
Steel tube	206	0.3		434.6	546.2	[21, 22]

E – elastic model, μ – Poisson's ratio, f_{ck} – concrete compressive strength

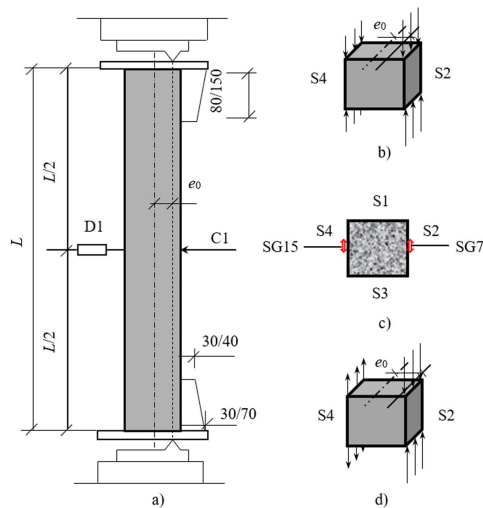


Fig. 1. Test set-up and the state of stress: a) Schematic representation of the specimen, b) state of stress under small γ values, c) arrangement of strain gauges, d) state of stress under large γ values

When $L = 450$ mm, the stiffener was considered to have either small values such as 30 mm and 80 mm or large values such as 70 mm and 150 mm. Figs. 1b and 1d show stress state under low and high RCFST column eccentric compressions, respectively. Fig.1(c)

shows surface (S) and strain gauge (SG) numbers at RCFST column central section. Further, S2 and S4 represent compressive and tensile column sides, respectively.

2.2. Test materials

The material properties of the RCFST specimens that were discussed in [21, 22] are illustrated in Table 1. The value of concrete elastic modulus E was calculated using $E_c = 3320\sqrt{f_{ck}} + 6900$ MPa on ACI 363R-92 [25].

2.3. Test results

In the present research, statistical analyses were performed on strain gauges 7 (SG7) and 15 (SG15) on surfaces 2 (S2) (compression side) and 4 (S4) (tension side), respectively (Fig. 1c). Fig. 2 shows the outer envelopes of RCFST column load-strain (P - ε) relationships exposed to eccentric compressive load for various λ and γ values.

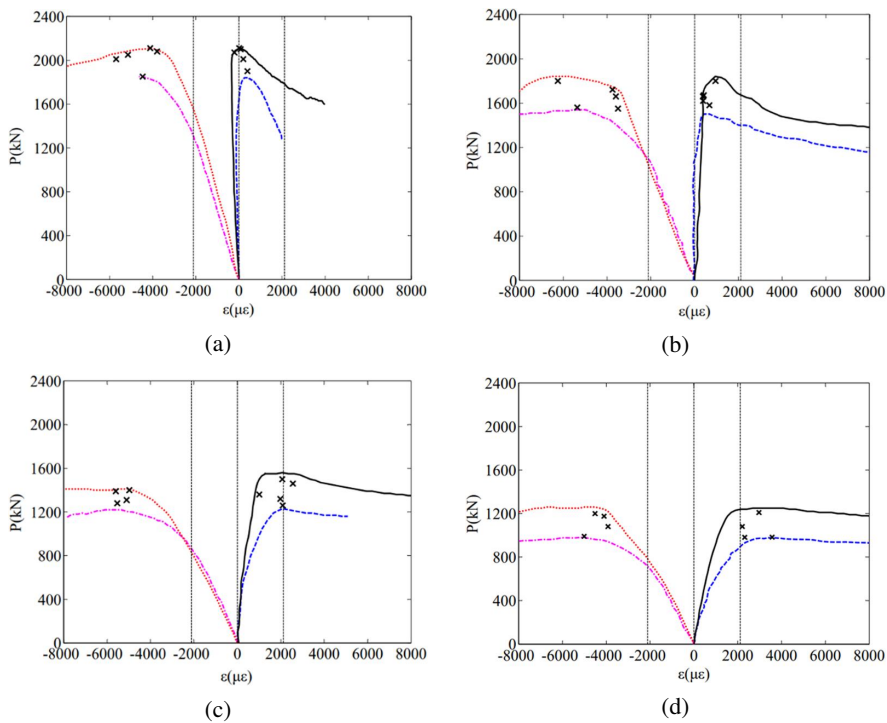


Fig. 2. P - ε curve of the RCFST: a) $\gamma = 0.13$, b) $\gamma = 0.23$, c) $\gamma = 0.33$, d) $\gamma = 0.43$

The peak loads of the test are listed in Table 2. From the analysis, it was observed that peak P value is decreased with the increase of γ . Further, RCFST system P - ε relationship revealed a linear to nonlinear material behavior until peak response followed by

Table 2. Information of 16 groups RCFST columns

No.	Specimen	L (mm)	λ	γ	$P_{u\text{test}}$ (kN)	$P_{u\text{FEa}}$ (kN)	$P_{u\text{cal}}$ (kN)	err _{FEa} (%)	err _{cal} (%)	Ref
1	EC1-1/2	450	10.4	0.13	2112	2215	2300	4.9	8.9	[22]
2	EC2-1/2	450	10.4	0.23	1782	1859	1939	4.3	8.8	[22]
3	EC3-1/2	450	10.4	0.33	1508	1557	1490	3.2	-1.2	[22]
4	EC4-1/2	450	10.4	0.43	1255	1280	1324	2.0	5.5	[22]
5	LEC1-1/2	1000	23.1	0.13	2149	2100	2142	-2.3	-0.3	[21]
6	LEC2-1/2	1000	23.1	0.23	1670	1745	1780	4.5	6.6	[21]
7	LEC3-1/2	1000	23.1	0.33	1387	1447	1331	4.3	-4.0	[21]
8	LEC4-1/2	1000	23.1	0.43	1149	1190	1090	3.6	-5.1	[21]
9	LEC5-1/2	1500	34.6	0.13	2063	2047	2015	-0.8	-2.3	[21]
10	LEC6-1/2	1500	34.6	0.23	1582	1617	1645	2.2	4.0	[21]
11	LEC7-1/2	1500	34.6	0.33	1315	1327	1301	0.9	-1.1	[21]
12	LEC8-1/2	1500	34.6	0.43	1093	1082	1083	-1.0	-0.9	[21]
13	LEC9-1/2	2000	46.2	0.13	1851	1910	1860	3.2	0.5	[21]
14	LEC10-1/2	2000	46.2	0.23	1492	1593	1505	6.8	0.9	[21]
15	LEC11-1/2	2000	46.2	0.33	1200	1315	1120	9.6	-6.7	[21]
16	LEC12-1/2	2000	46.2	0.43	993	1076	986	8.4	-0.7	[21]

$P_{u\text{test}}$ – the peak value of the experimental P - ε curves,

$P_{u\text{FEa}}$ – the peak value of the FE analysis P - Δ curves,

$P_{u\text{cal}}$ – the peak value of the theoretical calculation, err – the error between $P_{u\text{cal}}$ and $P_{u\text{test}}$

a parabolic softening phase. Furthermore, high ductility characteristics were displayed in follow-up process with gradual decrease of P value. However, it was also observed that at very high values of γ (0.43) for the extreme case considered in the current research, RCFST long column was equivalent to a pure bending member. Further, compression (SG7) and tension (S4) regional working states, under peak-load conditions were classified into yield, compression, and unilateral compression instability states on the basis of SG15 variations [21, 22]. For RCFST specimen unilateral compression instability with low γ and λ values, as depicted in Figs. 2a and b, SG7 value at P_u was negative and lower than ε_y . However, SG15 value was higher than ε_y . This indicates that CCC and steel tube were under collaborative stress and RCFST column was in unstable state with unilateral compression. From these results, it is observed that for the compression and tension yield states, when the value of γ was high, the values of SG15 for P_u were higher than or equal to ε_y (Fig. 2c and 2d). Therefore, one could conclude that tension regional steel tubes were under plastic tension. At this time, the S2 and S4 of steel tube yielded under compression and tension, respectively. In addition, RCFST was found to be on both sides of the yield instability mode. Hence, concrete and steel tube could not work simultaneously.

3. FE Analysis

3.1. General conditions

RCFST columns were analysed using ABAQUS FEA software. Steel tubes were simulated 4-node reduced-integration shell elements (S4R). 8-node hexahedral elements (C3D8) were utilized for concrete column modeling. Further, eccentric axial loading boundary conditions were determined with the enforced displacement at column top reference point. The simulation of RCFST end-rigid plates was performed using 4-node 3-D bilinear rigid quadrilateral element (R3D4) combining surface node DoFs on the two reference points positioned at the center of the lower and upper surfaces. At the bottom reference point, the DoFs remained constant to simulate the fixed end boundary conditions. However, at the top reference point, $0.03L$ displacement along the axis direction was applied to realize the goal of loading on the column with displacement. In this paper, the reference steel tensile test curve in [21, 22] complied with constitutive model developed by Han et al. [26], and the developed concrete damage plastic (CDP) constitutive model proposed by Han et al. [27] was also used in this paper.

3.2. Instability mode of RCFST

3.2.1. P - ϵ relationship for RCFST

Figure 3 presents the comparison of the P - ϵ curves of RCFST columns under the coupling effects of various eccentricity ratios γ and slenderness ratios λ . From the figure, it is observed that all the RCFST columns exhibited typically smooth strain-softening properties. This complied with the findings by Li et al. [21, 22]. The obtained results showed that, with an increase in λ in RCFST columns, peak P value decreased slightly.

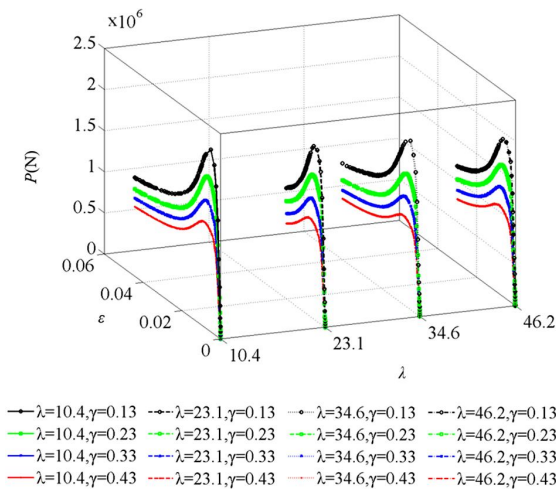


Fig. 3. P - ϵ curves under the coupling effects of γ and λ

However, $P-\varepsilon$ curves of various components revealed different characteristics for various γ . It was also found that an increase in γ significantly decreased the peak value of the yield steps on the $P-\varepsilon$ loss curves. The main reason for this was that γ , through the amplification of λ in the RCFST columns, decreased the total bearing capacity of the RCFST columns.

3.2.2. Instability state

In the process of the FE parametric analysis with L as the variable, the RCFST columns with various lengths showed similar instability modes. Therefore, the column with $L = 1500$ mm was selected as a typical case to show the analysis results. The distribution of the tensile damage factor (DAMAGET) of CCC under different γ values is featured in Fig. 4.

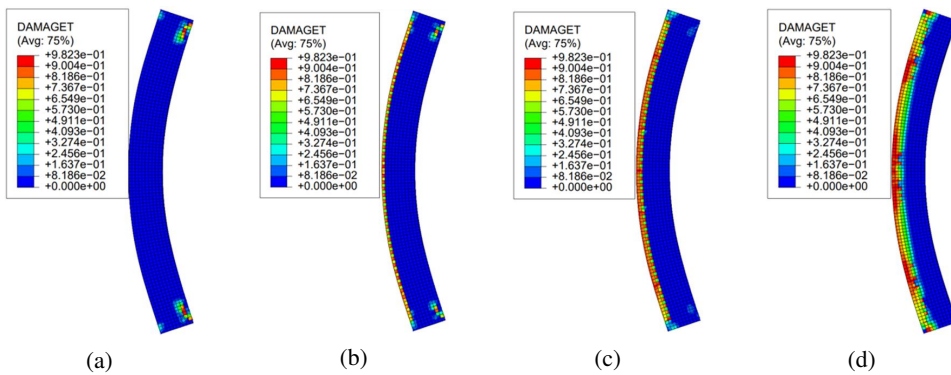


Fig. 4. DAMAGET of CCC: a) $\gamma = 0.13$, b) $\gamma = 0.23$, c) $\gamma = 0.33$, d) $\gamma = 0.43$

From Fig. 4a, it is observed that when γ was small ($= 0.13$), CCC only had cracks at both ends of the CCC column. This was mainly due to the uneven local stress of CCC caused by the eccentric pressure at the endplates, however, there was no damage inside the CCC column. Further, the penetrating damage region could not be formed in the CCC column and the bearing capacity of the column did not decrease rapidly. As presented in Figs. 4c and 4d, this explained the reason why the bearing capacity of the RCFST column with a small value of γ ($= 0.13$) was higher than those of other columns with higher γ values of 0.33 and 0.43.

Fig. 4b shows that when $\gamma = 0.23$, in addition to the local tensile damage at the endplates of the CCC column, the concrete at the tensile side of the column also had small-range damage. With an increase in the γ value to 0.33 and 0.43, the damage range of the CCC column changed from the endplates of the column to the longitudinal damage on the tensile side, and this damage range gradually spread to the center of the column as illustrated in Figs. 4c and 4d.

To explain the mentioned RCFST column instability process caused by steel tube stress and concrete compressive damage, longitudinal (S11) stresses of the steel tube at the central section of each specimen were displayed in Fig. 5 separately as the peak value in RCFST column $P-\varepsilon$ curves. From Fig. 5a, it is observed that when $\gamma = 0.13$, the steel tube was in

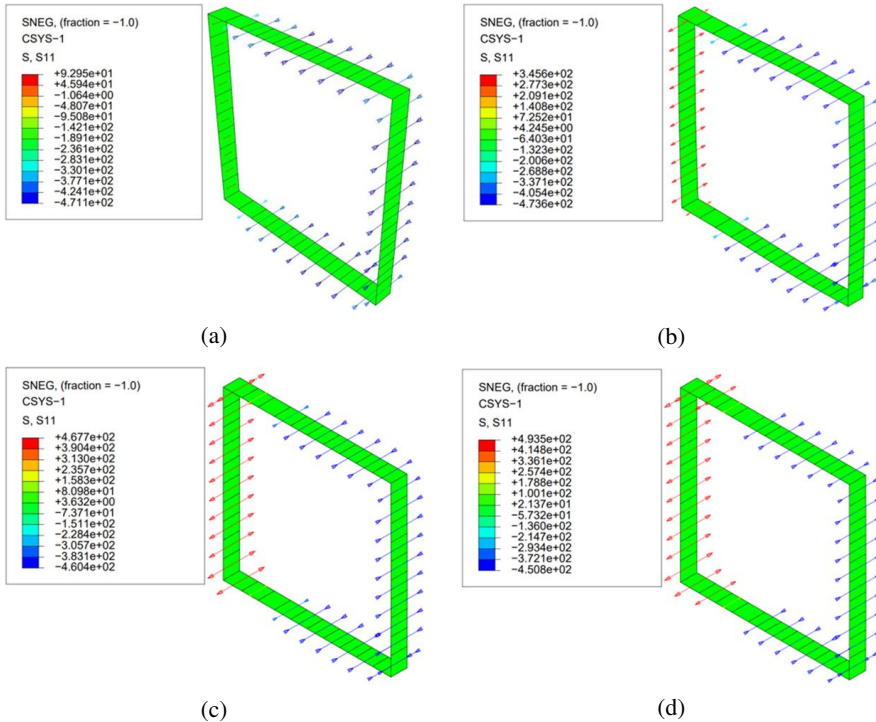


Fig. 5. Longitudinal stress of steel tube: a) $\gamma = 0.13$, b) $\gamma = 0.23$, c) $\gamma = 0.33$, d) $\gamma = 0.43$

the compressive state. Maximum longitudinal stress value on tensile side was +92 MPa and corresponding value on compressive side was -471 MPa. From Fig. 5, it is also observed that steel tubes on compression side were in compression yield state. From Fig. 5b, it is found that when $\gamma = 0.23$, the maximum values of the longitudinal stress on the tensile side was +346 MPa, and steel tube was under elastic tensile state. Further, on compressive side, maximum longitudinal stress value was found to be -473 MPa, and the steel tube was under compressive yield state. From Figs. 5c and 5d, when $\gamma = 0.33$ and 0.43, the steel tubes were found to be in the yield state on the tensile side. By increasing γ , tensile yield region extended beyond steel tube corner. Longitudinal stress was +468 MPa and +493 MPa, respectively. On the compression side, the steel tubes were in the yield state, and the longitudinal stress was -460 MPa and -451 MPa, respectively.

4. Mechanical analysis

FE analysis and experimental results revealed that the stability and strength (P_u) of RCFST columns were influenced by λ and γ coupling control. Based on whether tension side steel tube during instability process was in yield state or not, RCFST column instability

modes could be classified into two types, namely unilateral compression (Fig. 6a) and both sides yield instability modes (Fig. 6b).

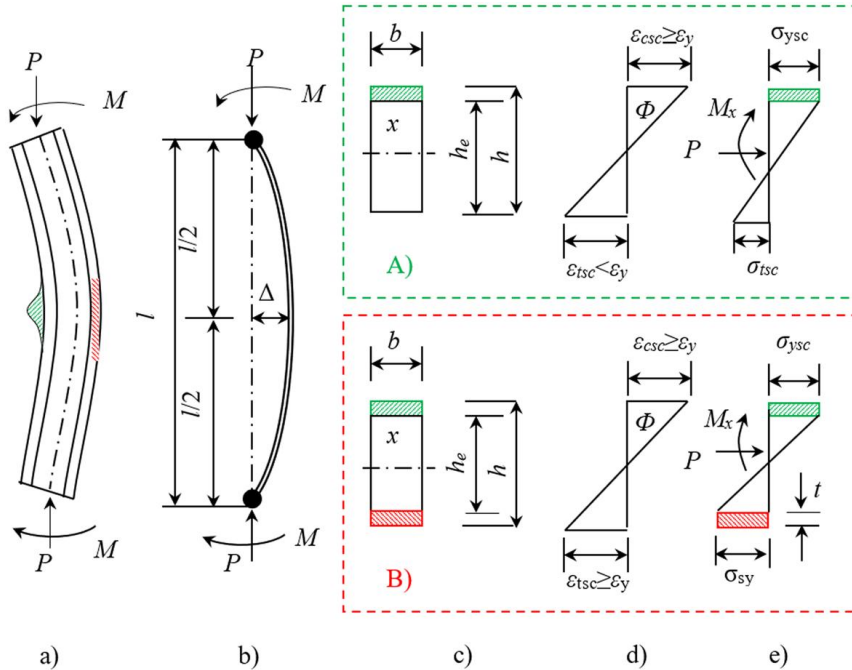


Fig. 6. RCFST column instability modes: A) unilateral compression, B) yield instability modes on both sides, a) phenomenon of instability, b) deformation curve, c) cross-sectional parameter, d) strain-state, e) stress-state

From $\gamma = \frac{e_0}{h}$, $\lambda = 2\sqrt{3}l/h$, it could be inferred that λ and γ influenced the interaction. Further, when λ and γ had low values, the development range of plastic yield was restricted to shaded portion in Figs. 6a and 6c, which were only on the compression side. Furthermore, a plastic yield zone appeared on both tension and compression sides when either γ or λ was high (Figs. 6b and 6c). In order to investigate the effect of λ and γ coupling on RCFST column stability, modified Jezeq analytical method was employed for the determination of RCFST column stability under eccentric compression when both ends were hinged.

4.1. Modified Jezeq's analytical method

Jezeq's method is a deflection analytical approach to solve the beam-column problems [28]. The solution was obtained using the following differential deflection as shown in Eq. (4.1) under various boundary conditions.

$$(4.1) \quad M'' - Py'' = q(x)$$

In Eq. (4.1), M refers to the bending moment, P refers to the axial load, y refers to the lateral deflection, q refers to the lateral load, and x refers to the longitudinal axis of the column. The original Jezek's method (1936) provided a closed-form solving method for an elastic-perfectly plastic column with rectangular cross-section under eccentric load beyond its elastic limit. The solution was obtained by solving Eq. (4.1) in three regions namely, elastic, primary plastic (yielding on column concave side), and secondary plastic (yielding on both convex and concave sides) regions. However, the theoretical foundation of the modified Jezek's analytical method in this paper was following: (1) CCC and steel tube could withstand compressive stress together under compression, while under tensile yield, steel tube could withstand tensile stress alone; CCC was not able to withstand tensile stress. (2) RCFST column deformation curve was in the form of a half-sine wave under eccentric load, as displayed in Fig. 6b.

The 16 groups of the RCFST columns samples of [21, 22] were divided into bending and compression members in biaxial symmetric rectangular section. The sectional area was calculated as $A = bh$ and the two ends were hinged. The two kinds of elastic-plastic instability modes that were under bending moment M and axial pressure P coupling action are as shown in Figs. 6a and 6b. In the case of RCFST column specimens with low γ values, yielding occurred only in compression zone, and central cross-section elastic zone height was h_e , as displayed in Figs. 6a and 6d. For samples with high γ , steel tubes in tension zone reached the yield strength f_{sy} while the compression zone reached yield strength, and elastic zone was shrunk to section middle, as depicted in Fig. 6a.

On the basis of the above two RCFST column instability modes, initially, the balance equations moment and load for the cross-section of middle height were derived and P - Δ relationship was determined. Afterwards, critical load P_u was determined according to extreme value condition as $\frac{dP}{d\Delta} = 0$. RCFST long column critical elastic load (P_E) was introduced in [27], as Eq. (4.2).

$$(4.2) \quad P_E = \frac{\pi^2 E_{sc} A_{sc}}{\lambda^2}$$

4.2. Unilateral compression instability mode of RCFST column

Figs. 6b and 6d show the diagram of strain distribution in RCFST column middle height section at low eccentric compression values, and Figs. 6b and 6e show corresponding stress distributions. In Eq. (4.3), P_y is RCFST column plastic yield-bearing load under axial compression, A refers to the sectional area. The load balance condition of column middle height section was achieved using Eq. (4.4).

$$(4.3) \quad P_y = \sigma_{y_{sc}} A$$

$$(4.4) \quad P = P_y - \frac{1}{2} (\sigma_{y_{sc}} + \sigma_{t_{sc}}) bh_e$$

The moment balance condition of middle height section was calculated using Eq. (4.5), and from Eqs. (4.3) and (4.4), Eq. (4.6) was obtained.

$$(4.5) \quad M + P\Delta = \frac{1}{2} (\sigma_{y_{sc}} + \sigma_{t_{sc}}) bh_e \left(\frac{h}{2} - \frac{h_e}{3} \right)$$

$$(4.6) \quad h_e = \frac{3h}{2} - \frac{3(M + P\Delta)}{P_y - P}$$

Based on modified Jezek analytical method second assumption, RCFST column deflection curve was obtained using Eq. (4.7). From the definition of \hat{O} , the result was obtained as shown in Eq. (4.8).

$$(4.7) \quad y = \Delta \sin \frac{\pi x}{l}$$

$$(4.8) \quad \Phi = -y'' \left(\frac{l}{2} \right) = \frac{\Delta \pi^2}{l^2} = \frac{2(P_y - P)}{E_{sc} bh_e^2}$$

After taking Eq. (4.6) into Eq. (4.8), middle height cross-section external and internal stresses were balanced, and deformation compatibility condition was transformed into $P-\Delta$ relationships, as stated in Eq. (4.9). From the critical equilibrium condition $\frac{dP}{d\Delta} = 0$, Eq. (4.10) was obtained.

$$(4.9) \quad \Delta \left(\frac{h}{2} \left(1 - \frac{P}{P_y} \right) - \frac{M + P\Delta}{P_y} \right)^2 = \frac{2l^2 P_y}{9b\pi^2 E_{sc}} \left(1 - \frac{P}{P_y} \right)^3$$

$$(4.10) \quad \Delta = \frac{P_y}{3P} \left(\frac{h}{2} \left(1 - \frac{P}{P_y} \right) - \frac{M}{P_y} \right)$$

By substituting Eq. (4.10) into Eq. (4.9) in order to obtain the peak value of eccentric compressive strength (P_u), Eq. (4.11) was obtained.

$$(4.11) \quad P_u = \frac{bh^3 \pi^2 E_{sc}}{12l^2} \left(1 - \frac{2M}{hP_y \left(1 - \frac{P_u}{P_y} \right)} \right)^3$$

In Eq. (4.11), $M = P_u e_0$. The following assumptions were made: $\alpha = \frac{P_u}{P_y}$, and $P_{E0} = \frac{\pi^2 E_{sc} bh^3}{12l^2}$ is long column Euler critical stress. Ideal steel elastic-plastic constitutive relation was modified based on RCFST λ with Eq. (4.2) to replace P_{E0} in Eq. (4.11). At this time, P_u was obtained using Eq. (4.12).

$$(4.12) \quad P_u = P_E \left(1 - \frac{2M}{hP_y(1 - \alpha)} \right)^3$$

Since M in Eq. (4.12) was also a function of P_u , Eq. (4.12) did not have an explicit solution and it was necessary to be solved through Newton interpolation method. In addition, λ was regularized as $\bar{\lambda}^2 = \frac{P_y}{P_E}$ [29], and then Eq. (4.12) was reduced to Eq. (4.13).

$$(4.13) \quad \alpha \bar{\lambda}^2 = \left(1 - \frac{2\alpha\gamma}{(1-\alpha)}\right)^3$$

The abovementioned equations were determined under $\sigma_{tsc} \leq f_{scp}$ and $\frac{h_e}{h} > 1 - \alpha$ conditions. According to Eq. (4.5) and Eq. (4.12), it was concluded as shown in Eq. (4.14).

$$(4.14) \quad \gamma < \frac{1-\alpha}{2}.$$

4.3. RCFST column both sides tension and compression yield instability modes

In both sides, yield instability modes of tension and compression, steel tube outer side was tensile yielded. During this time, the tension of steel tube was obtained as expressed in Eq. (4.15). External and internal stress balance conditions were determined using Eq. (4.16).

$$(4.15) \quad T = f_{sy}bt$$

$$(4.16) \quad P - \beta T = P_y - \frac{1}{2}(\sigma_{y_{sc}} + \sigma_{t_{sc}})bh_e$$

In Eq. (4.16), β refers to the coefficient of the longitudinal tensile strength of the steel tube. Steel tube tension on tensile side was not uniform, as illustrated in Figs. 3b–3d. Due to this reason, β was introduced to describe these characteristics.

$$(4.17) \quad \sigma_{y_{sc}} + \sigma_{t_{sc}} = \frac{2(P_y - P + \beta T)}{bh_e}$$

According to moment balance condition, Eq. (4.18) and Eq. (4.19) were inferred as:

$$(4.18) \quad M + P\Delta = \frac{\beta Th}{2} + \frac{1}{2}(\sigma_{y_{sc}} + \sigma_{t_{sc}})bh_e \left(\frac{h}{2} - \frac{h_e}{3}\right)$$

$$(4.19) \quad \Phi = -y'' \left(\frac{l}{2}\right) = \frac{\Delta\pi^2}{l^2} = \frac{\varepsilon_{y_{sc}} + \varepsilon_{t_{sc}}}{h_e} = \frac{\sigma_{y_{sc}} + \sigma_{t_{sc}}}{E_{sc}h_e} = \frac{2(P_y - P + \beta T)}{E_{sc}bh_e^2}$$

From the critical equilibrium condition $\frac{dP}{d\Delta} = 0$, Eq. (4.20) was obtained. By assuming that $\frac{\beta T}{P_y} = \eta$, Eq. (4.20) was reduced to Eq. (4.21).

$$(4.20) \quad P_u = P_E \left(1 - \frac{2M + \beta Th}{hP_y \left(1 - \frac{P}{P_y} - \frac{\beta T}{P_y}\right)}\right)^3$$

$$(4.21) \quad \alpha \bar{\lambda}^2 = \left(1 - \frac{2\alpha\gamma + \eta}{1 - \alpha - \eta}\right)^3$$

The above equations were derived under $\sigma_{tsc} \geq \sigma_{yyc}$ and $\frac{h_e}{h} \leq 1 - \alpha$ conditions. According to Eq. (4.6), the following results were obtained as shown in Eq. (4.22).

$$(4.22) \quad \alpha \geq 1 - (1 - \alpha + \eta)^2 - 2\alpha\gamma + 2\eta$$

On the basis of the Newton interpolation method, Maple program was employed to determine P_u in the two instability modes.

The following program flow was applied which was similar to [30] as follows:

Step 1: Solve Eq. (4.1)–(4.10) with A_c , A_s , f_{ck} , f_{sy} to receive P_E and P_y ;

Step 2: Initialize to set $P_u = 0.5P_y$;

Step 3: Determine whether $\gamma < (1 - \alpha)/2$ is true if it is true solve Eq. (4.12) to receive P_u ; else solve Eq. (4.15) to receive T , after that solve Eq. (4.20) to receive P_u .

RCFST column mechanical and physical indexes and geometric parameters are illustrated in Tables 1 and 2. A comparison was made between calculation results and RCFST column samples under λ and γ coupling action in [21, 22]. The findings were summarized in Table 1. In Table 1, it is seen that the calculation program and formula developed in the current research could ensure that the differences between analytical results and specimens were in the range of 10%, which meets detailed design requirements of RCFST columns. From Eq. (4.12) and Eq. (4.20), relations could be found among P_u and the cube of γ and the square of λ , so γ effect on P_u was higher than the weight of λ . This could be validated using the analytical findings given in Table 2.

5. Conclusions

In this paper, the instability modes in the RCFST column were classified into two categories based on steel tube tension side yield states. Relevant P - ε curve relation was investigated for every RCFST column using experimental and numerical methods. The modified Jezek analytical method was proposed on Maple program to determine RCFST column P_u under different instability modes. The following conclusions were drawn from results obtained from this work:

1. γ had stronger effect than λ on P - ε curve peak value of RCFST long column. The high eccentricity γ was one of the reasons for the sharp reduction of P - ε curve peak value of RCFST columns during compressive loading. This enabled RCFST columns to achieve greater nonlinear features before softening and lower residual strength after softening.
2. The instability modes of RCFST column were classified into two categories according to whether steel tube tensile side yielded under different γ . At lower eccentricities, e.g. $\gamma = 0.13$ or 0.23 , RCFST long column instability mode was unilateral compression, while at high eccentricities, e.g. $\gamma = 0.33$, and 0.43 , RCFST long column instability mode was both sides yield instability modes.

3. The calculated λ for RCFST column was transformed into a composite material, and Euler critical stress determined according to ideal elastic-plastic steel body was interchanged with composite material, which enabled the possibility of the analytical calculation of instability modes of RCFST column.
4. Yield stress ratio on steel tube tensile side to the plastic yield strength of RCFST column full section was applied in order to transform the two RCFST column instability modes into dimensionless normalization equations. This not only expands Jezek analytical method application scope in determining the instability of RCFST columns, but also reveals that analytical calculation error was below 10% through comparison with many reference sample groups in [21, 22].

References

- [1] L.H. Han, W. Li, R. Bjorhovde, "Developments and advanced applications of concrete-filled steel tube (CFST) structures: Members", *Journal of Constructional Steel Research*, 2014, vol. 100, pp. 211–228, DOI: [10.1016/j.jcsr.2014.04.016](https://doi.org/10.1016/j.jcsr.2014.04.016).
- [2] L.H. Han, Y.J. Li, F.Y. Liao, "Concrete-filled double skin steel tube (CFDST) columns subjected to long-term sustained loading", *Thin-Walled Structures*, 2011, vol. 49, no. 12, pp. 1534–1543, DOI: [10.1016/j.tws.2011.08.001](https://doi.org/10.1016/j.tws.2011.08.001).
- [3] A. Kuranovas, D. Goode, A.K. Kvedaras, S.T. Zhong, "Load-bearing capacity of concrete-filled steel columns", *Journal of Civil Engineering and Management*, 2009, vol. 15, no. 1, pp. 21–33, DOI: [10.3846/1392-3730.2009.15.21-33](https://doi.org/10.3846/1392-3730.2009.15.21-33).
- [4] L.H. Han, C. Hou, Q.L. Wang, "Square concrete filled steel tube (CFST) members under loading and chloride corrosion: Experiments", *Journal of Constructional Steel Research*, 2012, vol. 71, no. 1, pp. 11–25, DOI: [10.1016/j.jcsr.2011.11.012](https://doi.org/10.1016/j.jcsr.2011.11.012).
- [5] Y.F. Yang, L.H. Han, X. Wu, "Concrete Shrinkage and Creep in Recycled Aggregate Concrete-Filled Steel Tubes", *Advances in Structural Engineering*, 2008, vol. 11, no. 4, pp. 383–396, DOI: [10.1260/136943308785836772](https://doi.org/10.1260/136943308785836772).
- [6] Z. Tao, L.H. Han, "Behaviour of fire-exposed concrete-filled steel tube beam columns repaired with CFRP wraps", *Thin-Walled Structures*, 2007, vol. 45, no. 1, pp. 63–76, DOI: [10.1016/j.tws.2006.11.004](https://doi.org/10.1016/j.tws.2006.11.004).
- [7] H.Y. Dong, Y.N. Li, W.L. Cao, Q.Y. Qiao, R.J. Li, "Uniaxial compression performance of rectangular CFST columns with different internal construction characteristics", *Engineering Structures*, 2018, vol. 176, pp. 763–775, DOI: [10.1016/j.engstruct.2018.09.051](https://doi.org/10.1016/j.engstruct.2018.09.051).
- [8] U.M. Sulthana, S.A. Jayachandran, "Experimental studies on the global stability of concrete sandwiched double steel tubular columns", *Advanced Steel Construction*, 2020, vol. 16, no. 2, pp. 99–111, DOI: [10.18057/IJASC.2020.16.2.2](https://doi.org/10.18057/IJASC.2020.16.2.2).
- [9] C. Guo, Z.R. Lu, "Effect of circumferential gap on dynamic performance of CFST arch bridges", *Journal of Bridge Engineering*, 2021, vol. 26, no. 2, art. ID 04020121, DOI: [10.1061/\(ASCE\)BE.1943-5592.0001661](https://doi.org/10.1061/(ASCE)BE.1943-5592.0001661).
- [10] Y.Q. Huang, J.Y. Fu, A.R. Liu, Y.L. Pi, D. Wu, W. Gao, "Effect of concrete creep on dynamic stability behavior of slender concrete filled steel tube column", *Composites Part B: Engineering*, 2019, vol. 157, pp. 173–181, DOI: [10.1016/j.compositesb.2018.08.117](https://doi.org/10.1016/j.compositesb.2018.08.117).
- [11] V.I. Patel, "Analysis of uniaxially loaded short round-ended concrete-filled steel tubular beam-columns", *Engineering Structures*, 2020, vol. 205, art. ID 110098, DOI: [10.1016/j.engstruct.2019.110098](https://doi.org/10.1016/j.engstruct.2019.110098).
- [12] *Eurocode 4: Design of Composite Steel and Concrete Structures-Part 1-1: General Rules and Rules for Buildings*. European Committee for Standardization, Brussels, 2004.
- [13] *ANSI/AISC 360-16 Specification for Structural Steel Buildings*. American Institute of Steel Construction, Chicago-Illinois, 2016.
- [14] *GB 50936-2014 Technical Code for Concrete Filled Steel Tube Structures*. Ministry of Housing and Urban-Rural Development of the People's Republic of China, China Architecture & Building Press, Beijing, 2014.

- [15] Y.X. Hua, L.H. Han, Q.L. Wang, C. Hou, "Behaviour of square CFST beam-columns under combined sustained load and corrosion: Experiments", *Thin-Walled Structures*, 2019, vol. 136, pp. 353–366, DOI: [10.1016/j.tws.2018.12.037](https://doi.org/10.1016/j.tws.2018.12.037).
- [16] Y.Y. Wang, Y. Geng, J. Chen, M.Z. Zhao, "Testing and analysis on nonlinear creep behaviour of concrete-filled steel tubes with circular cross-section", *Engineering Structures*, 2019, vol. 185, pp. 26–46, DOI: [10.1016/j.engstruct.2019.01.065](https://doi.org/10.1016/j.engstruct.2019.01.065).
- [17] C. Guo, Z.R. Lu, "Effect of temperature on CFST arch bridge ribs in harsh weather environments", *Mechanics of Advanced Materials and Structures*, 2020, pp. 1–16, DOI: [10.1080/15376494.2020.1790701](https://doi.org/10.1080/15376494.2020.1790701).
- [18] F.Y. Liao, L.H. Han, S.H. He, "Behavior of CFST short column and beam with initial concrete imperfection: Experiments", *Journal of Constructional Steel Research*, 2011, vol. 67, no. 12, pp. 1922–1935, DOI: [10.1016/j.jcsr.2011.06.009](https://doi.org/10.1016/j.jcsr.2011.06.009).
- [19] Z.R. Lu, C. Guo, G.C. Li, "Air void and ring gap effect on CFST arch bridges dynamic performance", *Journal of Constructional Steel Research*, 2021, vol. 177, art. ID 106418, pp. 1–14, DOI: [10.1016/j.jcsr.2020.106418](https://doi.org/10.1016/j.jcsr.2020.106418).
- [20] A.Y. Al-Attraqchi, M.J. Hashemi, R. Al-Mahaidi, "Hybrid simulation of bridges constructed with concrete-filled steel tube columns subjected to horizontal and vertical ground motions", *Bulletin of Earthquake Engineering*, 2020, vol. 18, pp. 4453–4480, DOI: [10.1007/s10518-020-00871-7](https://doi.org/10.1007/s10518-020-00871-7).
- [21] G.C. Li, B.W. Chen, Z.J. Yang, Y.P. Liu, Y.H. Feng, "Experimental and numerical behavior of eccentrically loaded square concrete-filled steel tube long columns made of high-strength steel and concrete", *Thin-Walled Structures*, 2021, vol. 159, art. ID 107289, DOI: [10.1016/j.tws.2020.107289](https://doi.org/10.1016/j.tws.2020.107289).
- [22] G.C. Li, B.W. Chen, Z.J. Yang, Y.H. Feng, "Experimental and numerical behaviour of eccentrically loaded high strength concrete filled high strength square steel tube stub columns", *Thin-Walled Structures*, 2018, vol. 127, pp. 483–499, DOI: [10.1016/j.tws.2018.02.024](https://doi.org/10.1016/j.tws.2018.02.024).
- [23] S.M. Zhang, L.H. Guo, Z.L. Ye, Y.Y. Wang, "Behavior of steel tube and confined high strength concrete for concrete-filled RHS tubes", *Advances in Structural Engineering*, 2005, vol. 8, no. 2, pp. 101–116, DOI: [10.1260/1369433054037976](https://doi.org/10.1260/1369433054037976).
- [24] L.H. Han, G.H. Yao, "Experimental behaviour of thin-walled hollow structural steel (HSS) columns filled with self-consolidating concrete (SCC)", *Thin-Walled Structures*, 2004, vol. 42, no. 9, pp. 1357–1377, DOI: [10.1016/j.tws.2004.03.016](https://doi.org/10.1016/j.tws.2004.03.016).
- [25] ACI 363R-92 *State-of-the-art Report on High-strength Concrete*. Detroit, 1997.
- [26] L.H. Han, G.H. Yao, Z. Tao, "Performance of concrete-filled thin-walled steel tubes under pure torsion", *Thin-Walled Structures*, 2007, vol. 45, no. 1, pp. 24–36, DOI: [10.1016/j.tws.2007.01.008](https://doi.org/10.1016/j.tws.2007.01.008).
- [27] L.H. Han, G.H. Yao, X.L. Zhao, "Behavior and calculation on concrete-filled steel CHS (Circular Hollow Section) beam-columns", *Steel and Composite Structures*, 2004, vol. 4, no. 3, pp. 169–188, DOI: [10.12989/scs.2004.4.3.169](https://doi.org/10.12989/scs.2004.4.3.169).
- [28] C.C. Weng, C.P. Lin, "Study on maximum strength of cold-formed steel columns", *Journal of Structural Engineering*, 1992, vol. 118, no. 1, pp. 128–146, DOI: [10.1061/\(ASCE\)0733-9445\(1992\)118:1\(128\)](https://doi.org/10.1061/(ASCE)0733-9445(1992)118:1(128)).
- [29] J.M. Portolés, M.L. Romero, F.C. Filippou, J.L. Bonet, "Simulation and design recommendations of eccentrically loaded slender concrete-filled tube columns", *Engineering Structures*, 2011, vol. 33, no. 5, pp. 1576–1593, DOI: [10.1016/j.engstruct.2011.01.028](https://doi.org/10.1016/j.engstruct.2011.01.028).
- [30] Y. Bouras, Z. Vrcelj, "Thermal in-plane stability of concrete-filled steel tube arches", *International Journal of Mechanical Sciences*, 2019, vol. 163, art. ID 105130, DOI: [10.1016/j.ijmecsci.2019.105130](https://doi.org/10.1016/j.ijmecsci.2019.105130).